**Batteries & Supercaps**

Review
doi.org/10.1002/batt.202400071

Chemistry
Europe
European Chemical
Societies Publishing

www.batteries-supercaps.org
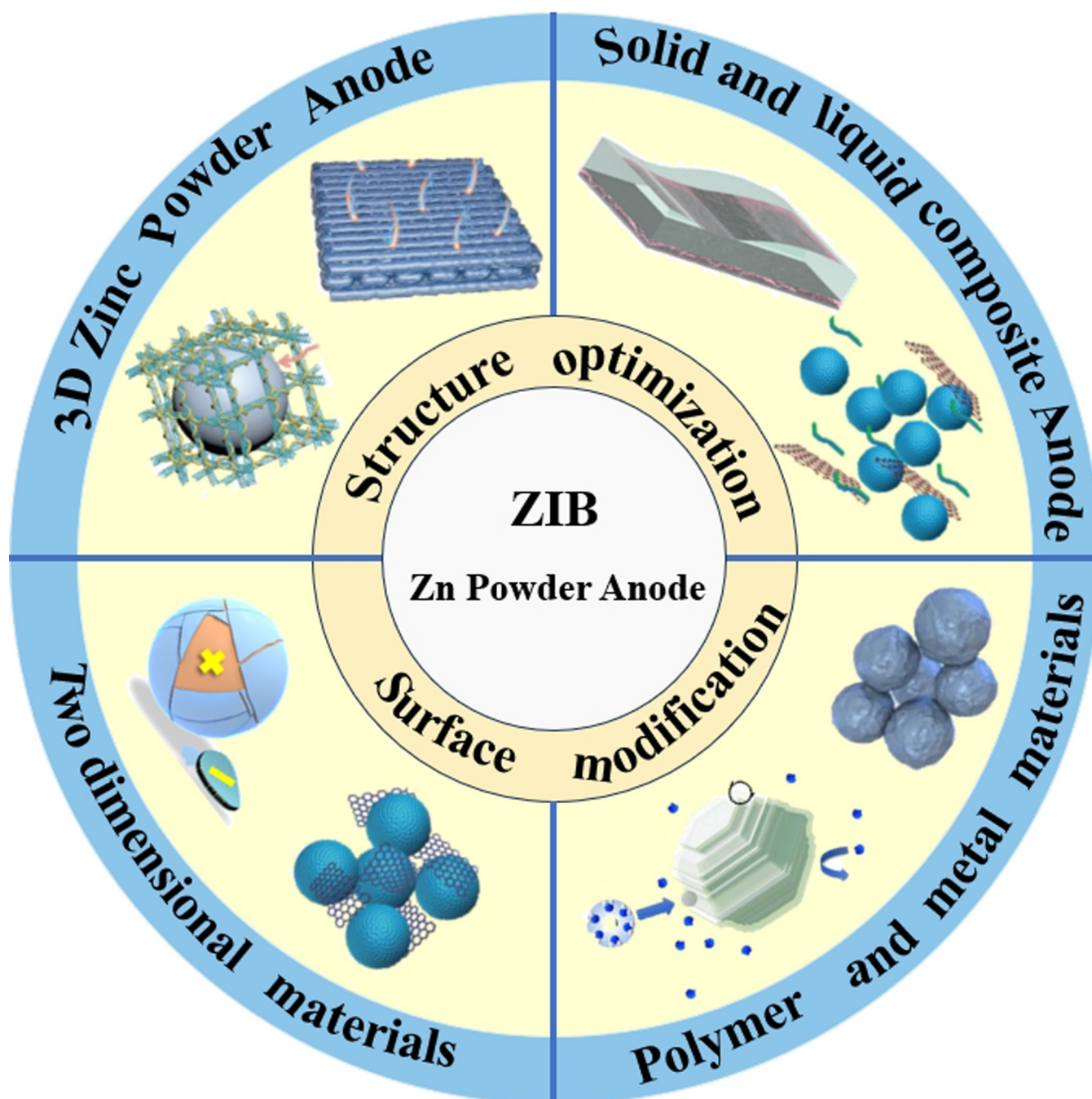
# Harnessing the Potential of Zn Powder Anodes: Innovations and Future Directions in Aqueous Zinc-Ion Batteries

Dongshu Liu,[a] Xilian Xu,*[c] Shibo Meng,[a] Jun Li,[c] Jinxiu Feng,[a] Yuchao Chen,[a] Wenxian Liu,[a] Fangfang Wu,[a] Wenhui Shi,*[b] and Xiehong Cao*[a]

**Batteries & Supercaps**

Review
doi.org/10.1002/batt.202400071

Chemistry
Europe

European Chemical
Societies Publishing

The pursuit of alternative anode materials featuring inexpensive, efficient, and adaptable is shaping the future of rechargeable zinc-ion batteries. The Zn powder anodes stand out among contenders due to their cost-effectiveness, exceptional processability, and adjustability. However, their widespread use is hampered by significant challenges, including volume expansion and dendrite growth. To counter these issues, a gamut of optimization strategies for Zn powder anodes has been explored and developed. This review systematically encapsulates these research findings, offering a comprehensive understanding of various enhancement methods, such as three-dimensional printing, in-situ surface engineering, scalable electrostatic self-assembly, and epoxy oligomer binding. These methodologies are discussed in detail in the context of their unique synthesis methods and underlying mechanisms. The paper concludes by outlining prospective research trajectories aimed at further optimizing the use of Zn powder anodes in aqueous zinc-ion batteries, thereby illuminating potential avenues for future exploration and development.

## 1. Introduction

The growing demand for energy with the increasing environmental pollution have prompted us to develop clean and renewable energy production technologies, such as wind, tidal and solar energy.[1,2] However, the uneven regional distribution and intermittent nature of these resources present significant challenges.[3,4] This makes low-cost, high-safety, environmentally friendly energy storage devices indispensable.[5–7] Leveraging the merits of abundant natural reserves, affordable cost, high theoretical capacity (820 mAg$^{-1}$ and 5855 mAhcm$^{-3}$), the low redox potential ($-0.76$ V vs. SHE) of metallic zinc, aqueous zinc batteries (AZBs) with metallic zinc as anode has been considered as a promising energy storage device.[8–11] Since the invention of rechargeable zinc–nickel (Zn–Ni) battery system, zinc anodes have been regarded as the ideal negative electrode for various rechargeable zinc-based battery system, such as Zn–Ni, Zn–MnO$_2$, Zn–air, Zn-ion batteries.[12,13] Among them, the aqueous Zn-ion batteries (ZIBs) using neutral/weakly acidic electrolytes systems have received strong attention in recent years.[14–16]

In the ZIBs system, the reaction of Zn anode primarily consists of two main steps: i) the transfer of electrons from Zn metal anode to the cathode via the external circuit, and ii) the oxidation of Zn to Zn$^{2+}$ ions, which subsequently diffuse to the cathode through the electrolyte.[17,18] However, challenges arise due to the uneven plating/striping behavior of Zn during charge and discharge, leading to numerous protrusions on the surface of commonly used Zn anodes.[19,20] In acidic/mild electrolyte systems, a series of side reactions contribute to the formation of zinc hydroxide sulfate (ZHS), zinc oxide or other zinc compounds, which passivate the surface of the zinc anode.[21–24] These issues significantly hinder the large-scale practical application of ZIBs in energy storage systems.

Recently, numerous strategies such as surface/interface modification,[25] structural design,[26,27] have been employed to improve the stability of Zn anodes. However, in most reports, planar Zn foils are utilized as both the current collector and the active material.[28] Moreover, the considerable weight of the currently used Zn foil leads to resource wastage and compromises the energy density of ZIBs. As a candidate for Zn anodes in practical industrial applications, Zn powder offers unique advantages over planar zinc foils, including cost-effectiveness, adjustability, and versatility (Figure 1a).[29–31] Specifically, the use of Zn powder based anodes can tremendously improve the utilization rate of Zn anodes, thereby enhancing the overall volumetric energy density.[32] As the development of novel Zn powder materials and their innovative design strategies continues (Figure 1b), some of the previous reviews on the progress of zinc anodes have not encompassed them. In this paper, the latest developments of Zn powder anode modification strategies are systematically summarized, with a particular focus on surface modification and structural design. We will discuss the key role of these modification strategies in inhibiting volume expansion, dendrite growth, and hydrogen evolution. Finally, the challenges and future research directions are proposed.

## 2. Main Challenges for Zn Powder Anodes

Volume expansion, Surface corrosion, dendrite growth and hydrogen evolution reaction (HER) are the main factors affecting the practical application of Zn powder anodes (Figure 2).[33,34] Characterized by a unique spherical microstructure and a large surface area, Zn powder anodes face drastic volume changes during the cycling.[35] As a result, the Zn powder gradually loses contact with the current collector, possibly leading to detachment, and ultimately causing a short circuit in the battery. Additionally, the ion redistribution path of Zn powder is elongated and irregular. Therefore, unlike the nucleation mechanism observed in isotropic two-dimensional Zn foil, the deposition behavior of three-dimensional Zn powder anodes is predominantly concentrated in the region of spherical tips with shorter transport paths.[36–38] During deposition, zinc atoms preferentially return to these nuclei at the spherical tips, triggering the formation of "spikes" and facilitating excessive growth of Zn dendrites.[39] At higher current

[a] D. Liu, S. Meng, J. Feng, Y. Chen, W. Liu, F. Wu, Dr. X. Cao
College of Materials Science and Engineering
Zhejiang University of Technology
18 Chao wang Road, Hangzhou 310014, China
E-mail: gcscaoxh@zjut.edu.cn

[b] Dr. W. Shi
Center for Membrane and Water Science & Technology
College of Chemical Engineering
Zhejiang University of Technology
18 Chao wang Road, Hangzhou 310014, China
E-mail: shiwh@zjut.edu.cn

[c] Dr. X. Xu, J. Li
Alphaverse Grp Ltd, Hong Kong 999077, China
E-mail: xuxilian@zust.edu.cn
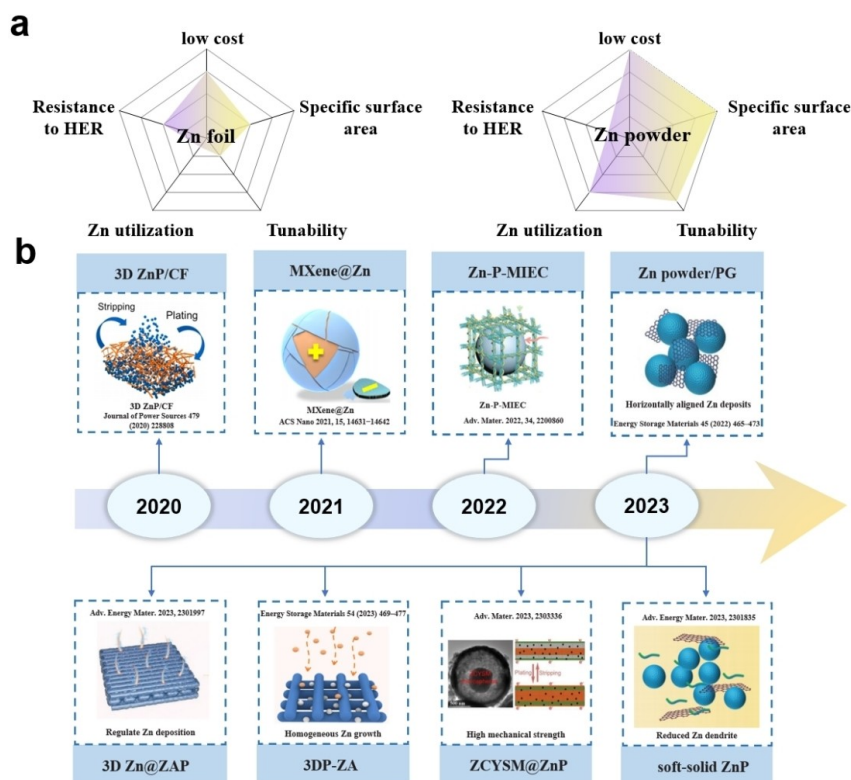
**Figure 1.** a) Comparative analysis of the advantages of Zn foil and Zn powder materials. b) Timeline of outstanding works in Zn powder anode research
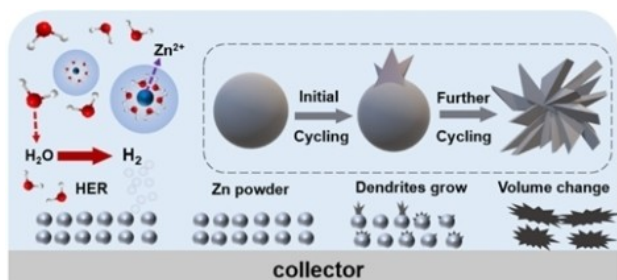


**Figure 2.** Schematic diagram of factors contributing to the degradation of Zn powder anode performance.

densities, the process of zinc deposition is significantly accelerated. The accumulation of electric charge on the zinc tip (also known as the "zinc tip effect") further enhances the growth of zinc dendrites. Consequently, this leads to a decrease in capacity and even breakdown of the separator, ultimately resulting in a short circuit. Additionally, the kinetics of hydrogen evolution is accelerated in aqueous electrolyte systems due to the larger specific surface area and enhanced accessibility to the active site.[40] Consequently, this will result in a more pronounced corrosion of the Zn powder anode compared to the two-dimensional Zn foil, potentially leading to structural collapse even in the case of a spherical Zn powder configuration.[34,41] The generation of $H_2$ leads to an accumulation of hydroxide ions on the surface of the Zn powder anode, thereby facilitating the formation of an irreversible by-product known as $ZnSO_4(OH)_6 \cdot xH_2O$ (ZHS). This phenomenon subse-
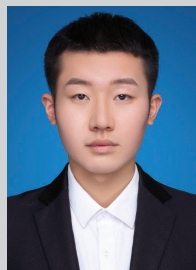
Dongshu Liu received a bachelor's degree in the Department of Science from Changchun University in 2021. Now, he is working as a master student in Prof. Cao's group in the Department of Materials Science and Engineering, Zhejiang University of Technology. His research interests focus on aqueous zinc-ion batteries.
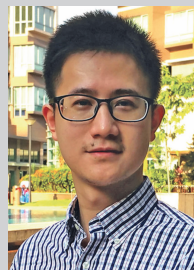


Prof. Xiehong Cao received his B.E. degree in polymer materials and engineering from Zhejiang University, China (2008), and then completed his Ph.D. under the supervision of Prof. Hua Zhang at the School of Materials Science and Engineering in Nanyang Technological University, Singapore (2012). After working as a research fellow in the same group, he joined Zhejiang University of Technology (China) in 2015 as a full professor. His current research interests include the synthesis of 2D nanomaterials and their applications in energy, the environment, etc..

quently contributes to an increase in internal resistance within the battery system, ultimately resulting in rapid battery failure.

Currently, numerous effective strategies have been developed to address the aforementioned problems of Zn powder anodes, involving structure design and surface optimization. The following section presents the latest progress on these strategies, illustrated with plenty of examples.

# 3. Surface Modification of Zn Powder Anode

According to the above analysis, improving the interface between anode and electrolyte and preventing direct contact between anode and water or oxygen in electrolyte is an effective way to inhibit dendrite growth and anode corrosion. Based on this, the surface modification strategy that has made some progress on Zn foil anodes seems to be a feasible approach. The strategy aims to improve the performance of the Zn anode by constructing different types of protective layers between the Zn anode and the aqueous electrolyte. Compared with two-dimensional Zn foil, Zn powder has more mature processing technology, which can simplify the process flow of surface modification strategy and reduce the cost, especially for large-scale preparation. Therefore, it is worth exploring to modify the anode surface of Zn powder to optimize the anode-electrolyte interface. Next, we will discuss recent advances in surface optimization strategies for Zn powder anodes, classified according to synthetic materials.

## 3.1. Two-dimensional Materials

MXene, a 2D transition metal carbide/nitride compound, possesses unique physical and chemical properties, such as good hydrophilicity, adjustable interlayer spacing and excellent electrical conductivity.[42] In recent years, multiple strategies for applying MXene as a zinc anode surface modification layer have been successfully validated.[43–45] Zhi and co-workers synthesized a MXene@Zn powder anode by using 2D MXene nanoflakes as a redistributor of electrons and ions through a electrostatic self-assembly method (Figure 3a).[39] The introduction of 2D MXene nanoflakes induced uniform $Zn^{2+}$ deposition while establishing a continuous electron transport channel. Because of the low lattice mismatch between Zn and MXene (Figure 3b, c), MXene@Zn powder anode has a low polarization voltage and stable cycle life. The assembled Zn‖FeHCF battery achieved a remarkable capacity retention rate of 77% after 1,000 cycles. Graphene is another typical 2D nanomaterial with excellent electrical conductivity. It has been successfully applied in Zn anodes to promote zinc deposition kinetics.[46–48] Li et al. used a multifunctional primitive graphene (PG) network to process zinc
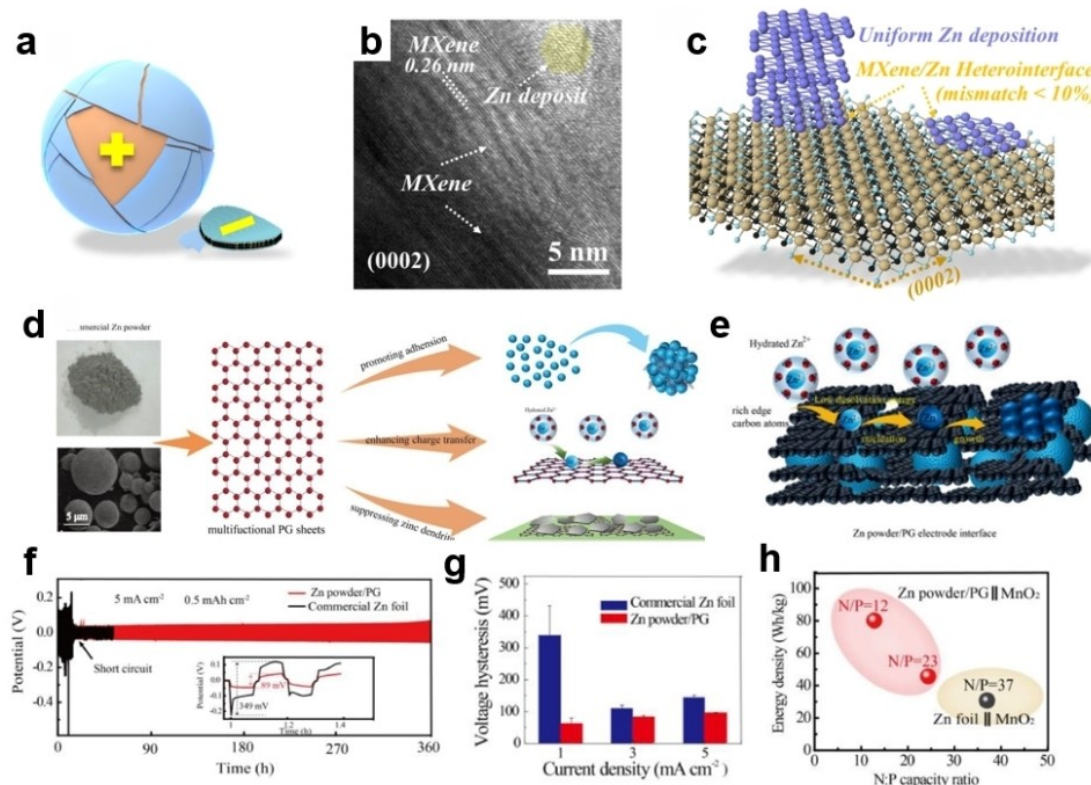


**Figure 3.** a) Schematic illustration of MXene@Zn anode. b) High-resolution transmission electron microscopy (HRTEM) image of MXene@Zn anode. c) Diagram depicting heterogeneous interfaces and uniform zinc deposits.[39] Copyright (2021) American Chemical Society. d) Schematic illustration of Zn powder/PG anodes. e) The schematic depiction of the deposition process of Zn powder/PG anodes. f) Voltage profiles of symmetric cells based on Zn powder/PG anodes. g) The average voltage hysteresis at different current densities. h) Energy density of the full battery with Zn powder/PG and Zn foil as anodes at different N/P ratios.[31] Copyright (2022) Elsevier.

**Batteries & Supercaps**

Review
doi.org/10.1002/batt.202400071

**Chemistry Europe**
European Chemical
Societies Publishing

powder into Zn powder anodes with high zinc utilization (Figure 3d, e).[31]

Thanks to the macro-assembly characteristics of PG tablets, loose Zn powder particles can be used to make electrodes (denoted as Zn powder/PG) without adding a PVDF binder. At a current density of 5 mA cm$^{-2}$, the voltage lag of the Zn powder/PG anode is much smaller than that of the zinc foil anode (349 mV), which was only 89 mV (Figure 3f, g). In addition, the weight energy density of the Zn||MnO$_2$ battery based on the Zn powder/PG anode was more than twice that of the Zinc foil anode with a lower N/P ratio (Figure 3h).

### 3.2. Polymer Materials

Polymers are promising alternatives for functional coatings on Zn anodes due to their inherent mechanical properties and active groups.[49–52] Various polymers have been successfully used a surface finishing coatings for zinc foil anodes. Theoretical analysis suggests that the polymer coating can accelerate the kinetics of Zn$^{2+}$ transport and promote the planar deposition of zinc.[53–55] Hou et al. prepared a polyethylene glycol-modified Zinc powder anode (denoted as Zn–P/PEG, Figure 4a).[56] Poly-

ethylene glycol can guide the growth of zinc along the (002) crystal surface during Zn deposition and inhibit the Zn–P/PEG anode side volume effect, hydrogen evolution, self-corrosion reactions (Figure 4b). At 5 mA cm$^{-2}$, the Zn symmetric cell could cycle for over 1000 h, while the Zn–P||Zn–P symmetric cell failed in less than 200 h (Figure 4c). In addition, the energy density of the complete battery using the Zn–p/PEG anode is also greatly improved (Figure 4d). Considering the volume change of Zn powder during the charge-discharge processes, polysilane, with Si–O–Si bond frameworks comes into sights. Qian et al. developed a polysilane modified protective layer functionalized by NH$_2$.[57] In this protective layer, the amino group can provide a strong interaction with Zn$^{2+}$, resulting in a uniform Zn flux. The Si–O–Zn bond is formed to ensure lasting bonding between the Zn powder anode and the protective layer. According to the DFT calculations, the binding energy of –NH$_2$ group is higher than that of –SH, –Cl and methyl groups. This indicates that NH$_2$–PSiOx can homogenize the Zn$^{2+}$ flux. Thus, Zn@NH$_2$–PSiOx powder anode showed superior electrochemical properties, lasting ~600 hours at 0.5 mA cm$^{-2}$ (Figure 4e, f).
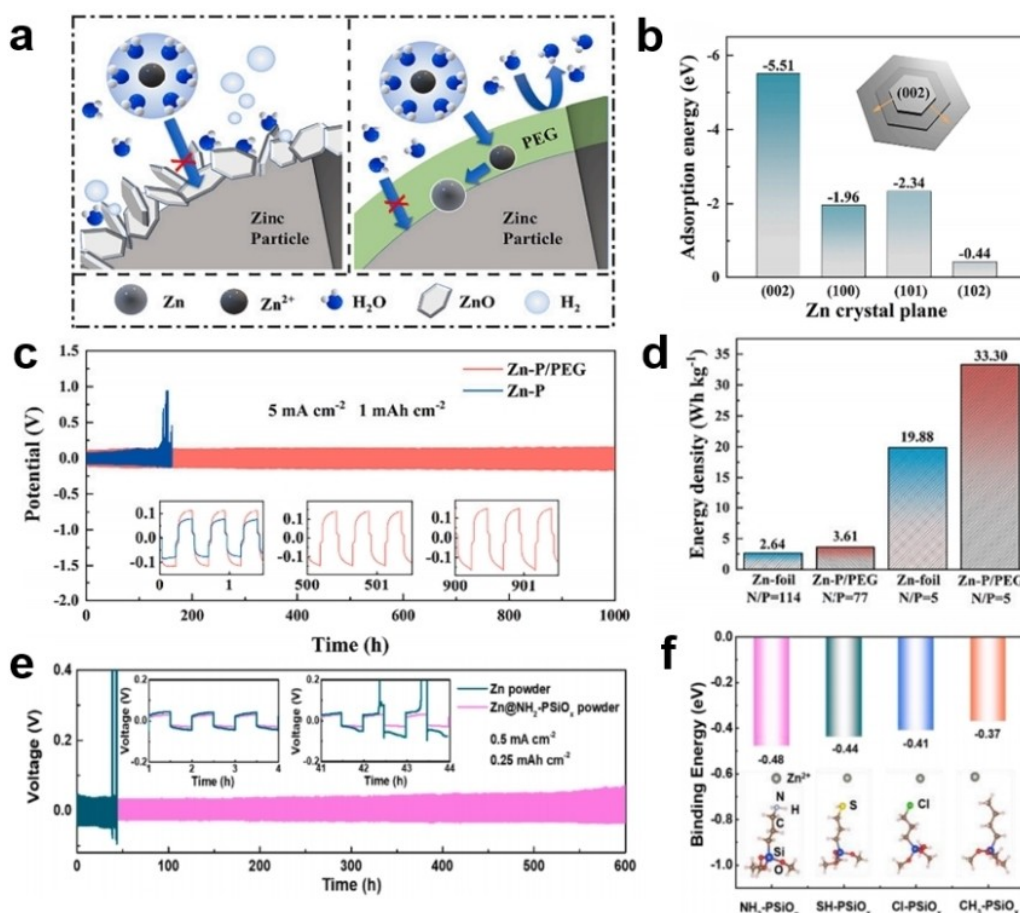


**Figure 4.** a) Diagram illustrating the action of polyethylene glycol on Zn powder surface. b) Adsorption energy of polyethylene glycol molecules on different crystal planes of Zn. c) Voltage profiles of symmetric cells based on Zn powder and Zn–P/PEG anodes. d) Energy density of the full battery with Zn–P/PEG and Zn-foil as anodes[56] Copyright (2023) Elsevier. e) Voltage profiles of symmetric cells based on Zn powder and Zn@NH$_2$–PSiOx powder anodes. f) Binding energies of silane molecules with different head groups to Zn.[57] Copyright (2023) Elsevier.

**Batteries & Supercaps**

Review
doi.org/10.1002/batt.202400071

**Chemistry Europe**
European Chemical
Societies Publishing

### 3.3. Metals

In addition to two-dimensional materials and polymers, some metals have also been applied to the surface modification of zinc anodes. Metals used as surface layers usually have excellent mechanical strength and corrosion resistance, such as Au, Ag, and Cu.[59–61] Based on this, Chen et al. proposed a modification strategy for metal indium, which has good corrosion resistance and higher hydrogen evolution overpotential, which can effectively alleviate the corrosion and hydrogen evolution phenomena of Zn powder anodes. The symmetric cells with Zn–P@In anode maintain a stable stripping/plating process for over 1400 h.[58] The surface modification strategy and their corresponding electrochemical properties are shown in Table 1.

## 4. Structural Optimization of Zn Powder Anode

Apart from constructing a surface protective layer, structural optimization of Zn anodes has emerged as an effective approach to address challenges related to Zn powder corrosions, Therefore, applying this strategy to Zn powder anodes, which offer superior processability and adjustability, is a smart tactic. In fact, the synthetic pathways optimized for Zn powder anode structures are simpler and more diverse. In this section, the structural design strategies of existing Zn powder anodes are summarized, with emphasis on the introduction of three-dimensional Zn powder anodes and solid-liquid composite Zn powder anodes.

### 4.1. 3D Structural optimization

In recent years, in order to improve the electrochemical performance of battery electrode materials, the concept of constructing conductive frames on electrode materials has been proposed.[62–65] One of the methods for designing 3D Zn powder anode structure is to introduce mixed ion conductive scaffold. Liang et al. successfully manufactured a flexible Zn powder anode with high conductivity, dendrite-free and corrosion resistance by using a hybrid ion electronic conductive scaffold (Figure 5a).[66] This structure allows the ZnP–MIEC anode to homogenize the $Zn^{2+}$ flux. Therefore, dendrite growth of the ZnP–MIEC anode is significantly inhibited even after 100 cycles (Figure 5b), and stable cycling is achieved at high rates (Figure 5c). This work provides a scalable approach for manufacturing efficient and reliable practical Zn powder anodes. In addition, biomimetic materials, due to their diverse uses and environmental friendliness, have found extensive applications in the field of rechargeable batteries and may bring about new breakthroughs in the development of Zn powder anodes.[67,68] Pang et al. have developed a high specific surface area Zn@C yolk shell microsphere (ZCYSM) film anode.[69] The ZCYSM@Zn powder anode based on this film demonstrated excellent electrical conductivity, cushioning, mechanical strength and corrosion resistance while regulating corrosion reaction and galvanizing/stripping. Compared with the volume effect in the discharge process of Zn powder anode, the yolk shell structure of ZCYSM@Zn anode can effectively limit the deposition of zinc metal in its interior, reduce the impedance and polarization potential of the Zn powder anode, thereby improving the utilization of the zinc powder anode and achieving a long cycle life of up to 4000 h (Figure 5d, e). In recent years, electrode designs with different gradients have enhanced zinc anode performance because local charge trans-

**Table 1.** Summary of the performance of Surface modified Zn powder anodes.

| Type | Anode | Working Mechanism | Average particle size of Zn powder | Cycle performance | Electrolyte | Full cell performance | Ref |
|---|---|---|---|---|---|---|---|
| Two-dimensional materials | Zn powder/PG | Uniform zinc deposits | / | 400 h at 1 mA cm$^{-2}$ 360 h at 5 mA cm$^{-2}$ | 2 M ZnSO$_4$ | 245 mAh g$^{-1}$ after100 cycles at 1 A g$^{-1}$ | [31] |
| | MXene@Zn | Uniform zinc deposits | ~5.0 μm | 200 h at 1 mA cm$^{-2}$ | 2 M ZnSO$_4$ | 77 % capacity retention after1000 cycles at 1 A g$^{-1}$ | [39] |
| | Zn_G | Uniform zinc deposits | / | 550 h at 1 mA cm$^{-2}$ | 2 M ZnSO$_4$ | 120 mAh g$^{-1}$ after1600 cycles at 0.5 A g$^{-1}$ | [29] |
| Polymer materials | Zn–P/PEG | Uniform zinc deposits | ~13.6 μm | 1000 h at 5 mAcm$^{-2}$ | 2 M ZnSO$_4$ | 88 % capacity retention after 100 cycles at 1 A g$^{-1}$ | [56] |
| | Zn@NH$_2$-PsiOx | Regulating the Zn$^{2+}$ flux. | / | 600 h at 0.5 mA cm$^{-2}$ | 2 M ZnSO$_4$ | / | [57] |
| Metal materials | Zn–P@In | Zn nuclei seeds | / | 1000 h at 1 mA cm$^{-2}$ | 2 M ZnSO$_4$ | 97.6 % capacity retention after 2000 cycles at 3 A g$^{-1}$ | [58] |
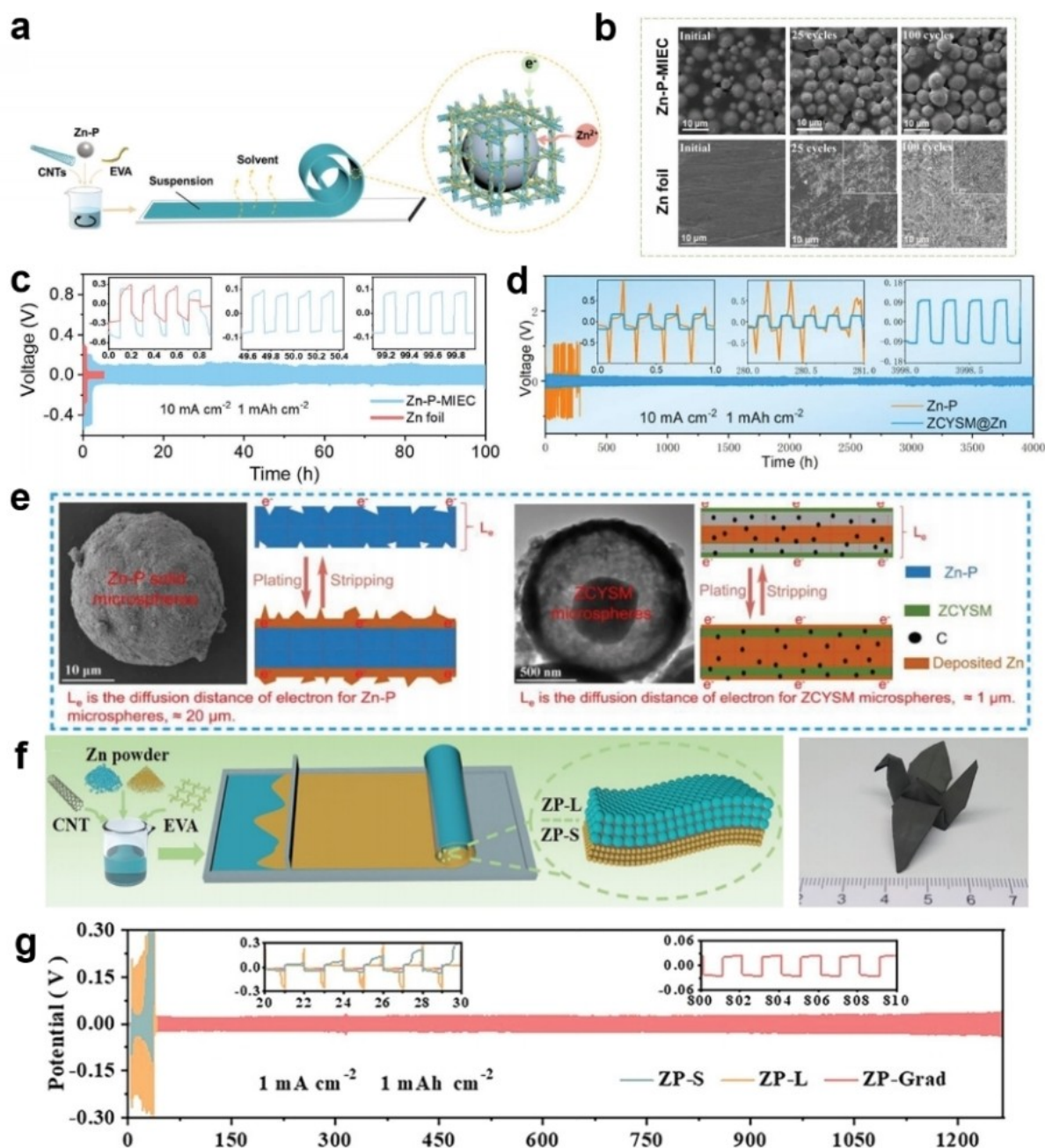
**Figure 5.** a) Schematic illustration of the Zn–P–MIEC fabrication process. b) SEM images of Zn–P–MIEC-based and Zn-foil-based symmetrical cells before and after cycles with a capacity of 0.05 mAh cm$^{-2}$. c) Voltage profiles of symmetric cells based on Zn foil and Zn–P–MIEC anodes.[66] Copyright (2022) John Wiley and Sons. d) Voltage-time profiles of Zn–P and ZCYSM@Zn symmetrical cells at a current density of 10 mA cm$^{-2}$ with a cycling capacity of 1 mAh cm$^{-2}$. e) Schematic illustration of Zn plating/stripping and cycling on Zn–P and ZCYSM microspheres.[69] Copyright (2023) John Wiley and Sons. f) Schematic diagram showing the preparation of the ZP-Grad anode. g) Voltage profiles of symmetric cells based on ZP–L, ZP–S, and ZP-Grad electrodes at a current densities of 1 mA cm$^{-2}$ with a cycling capacity of 1 mAh cm$^{-2}$[70] Copyright (2023) John Wiley and Sons.

port dynamics can be optimized efficiently. Due to its high gradient conductivity and porosity, the multi-gradient 3D electrode design strategy is considered to be a feasible path to improve electrode performance.[71–75] Guan's team reported a Zn powder anode with multiple gradients and pores (Figure 5f).[70] The Zn powder anode is conducive to the bottom-up deposition and stripping of zinc, and inhibits the dendrite growth of Zn powder. In addition, the pores in the Zn powder anode can reduce stress concentration and prevent the Zn powder

structure from collapsing. These advantages endow the flexible gradient Zn powder anode with cycle steadily for 1250 h at 1 mA cm$^{-2}$/1 mAh cm$^{-2}$ (Figure 5g). In recent years, 3D printing, as an emerging intelligent manufacturing technology, has been increasingly applied to the manufacturing of energy storage equipment components. This method can directly manufacture complex three-dimensional objects, such as electrodes and electrolytes in lithium-ion and sodium-ion battery systems, through solvent-based inks.[76–80] 3D printing allows for precise

control over the electrode geometry and thickness, and it can be fabricated with less time and materials.[81] Among the current mainstream 3D printing methods, direct writing printing stands out because of its low production cost, wide range of materials and convenient operation.[82–84] It is currently one of the 3D printing methods that have successfully realized practical applications in the field of energy storage devices.

This technology achieves a further increase in the specific surface area of the electrode material, which improves the conductivity of the electrode material, improves the electrode reaction kinetics, and allows a higher mass load of the active material.[87–89] Considering these advantages, the researchers propose this technology as an effective means to construct practical Zn powder anodes.

For example, Zhang's team built a porous zinc powder anode using a direct 3D printing method (Figure 6a).[85] The prepared 3DP-ZA anode has a large specific surface area and excellent electrochemical performance (Figure 6b). Benefiting from the specially designed porous structure and zinc-philic silver source customized through 3D printing, the 3D topographic image of the 3DP-ZA anode after circulation reveals a uniform coverage of Zn across its entire surface, without any abnormal local protrusions. In contrast, the Bulk-ZA anode exhibits numerous acicular bodies on its surface that aggregate into an uneven morphology, indicating non-uniform deposition behavior of zinc (Figure 6c). The 3DP-ZA anode can cycle for nearly 330 hours at $1 \, mA \, cm^{-2}$ and $1 \, mAh \, cm^{-2}$ (Figure 6d). In order to achieve a superior lifespan of the Zn powder anode at high current density/capacity, Guan and his colleagues reported a 3D printed zinc powder anode coated with a hydrogel (Figure 6e).[64] Cross-linked hydrogels can homogenize zinc ion flux and regulate the surface electric field of Zn powder anodes. In addition, the 3D structure of the 3D printing mitigated the volume change of the zinc powder anode during the cycle. The
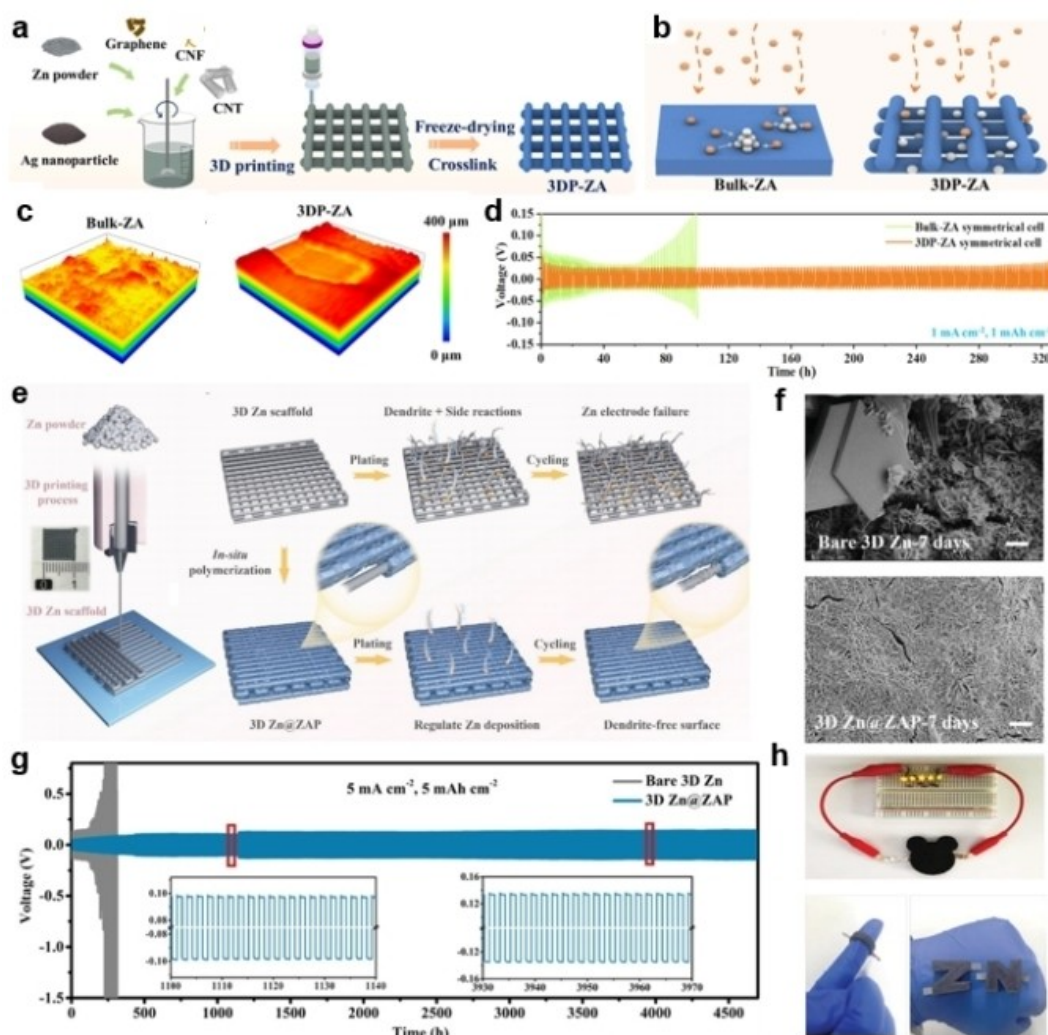


**Figure 6.** a) Schematic depiction of the 3DP-ZA anode fabrication process. b) Schematic illustration of 3DP-ZA anodes. c) the 3D topographic images of Bulk-ZA anodes and 3DP-ZA anodes after 10 cycles under a current density of $5 \, mA \, cm^{-2}$. d) Voltage profiles of symmetric cells based on Bulk-ZA and 3DP-ZA anodes.[85] Copyright (2023) Elsevier. e) The preparation process of the 3D Zn scaffold, and a comparative analysis of the Zn deposition mechanisms on bare 3D Zn and 3D Zn@ZAP anodes. f) SEM images of bare 3D Zn and 3D Zn@ZAP after immersion in 2 M $ZnSO_4$ electrolyte for 7 days. g) Voltage profiles of symmetric cells equipped with bare 3D Zn and 3D Zn@ZAP electrodes. h) Photographic images of the wearable 3D Zn@ZAP||$MnO_2$ cells on human body.[86] Copyright (2023) John Wiley and Sons.

**Batteries & Supercaps**

Review
doi.org/10.1002/batt.202400071

Chemistry
Europe
European Chemical
Societies Publishing

anode sample after soaking in 2 M $ZnSO_4$ electrolyte for 7 days, it was observed that the surface of 3D Zn@ZAP anode was smoother than that of ordinary bare 3D Zn anode, and there were no obvious large dendrites formed (Figure 6f). The obtained 3D Zn@ZAP symmetric battery owner has a cycle life of up to 4700 hours at 5 mA cm$^{-2}$ and 5 mAh cm$^{-2}$ (Figure 6g). Moreover, the full battery constructed from a 3D-printed Zn @ZAP anode and $MnO_2$ cathode can be seamlessly integrated with the human finger (Figure 6h). Furthermore, considering the production environment of the direct writing technology and the effect of temperature gradients on ink flow, Xu and co-workers developed a novel three-dimensional cold trap environment printing (3DCEP) technique to realize a 3DCEP-MXene/Zn

powder anode (Figure 7a).[90] 3DCEP technology improves the orientation stability of MXene nanosheets during the freezing process after ink extrusion (Figure 7b). In addition, the low lattice mismatch between MXene and Zn can effectively uniform zinc ion fluxes. Using these advantages, the 3DCEP-MXene/Zn powder anode can cycle stably for nearly 1400 hours (Figure 7c). In addition, the author also simulated the zinc ion flux distribution on the surface of Zn powder anode with COMSOL Multiphysics software and discussed the mechanism of uniform zinc deposition behavior with ordered orientation. Non-uniform deposition and growth of Zn occurred on the surface of 3DCEP−Zn−P anode during the charge-discharge cycle. On the contrary, when the oriented MXene is mixed with
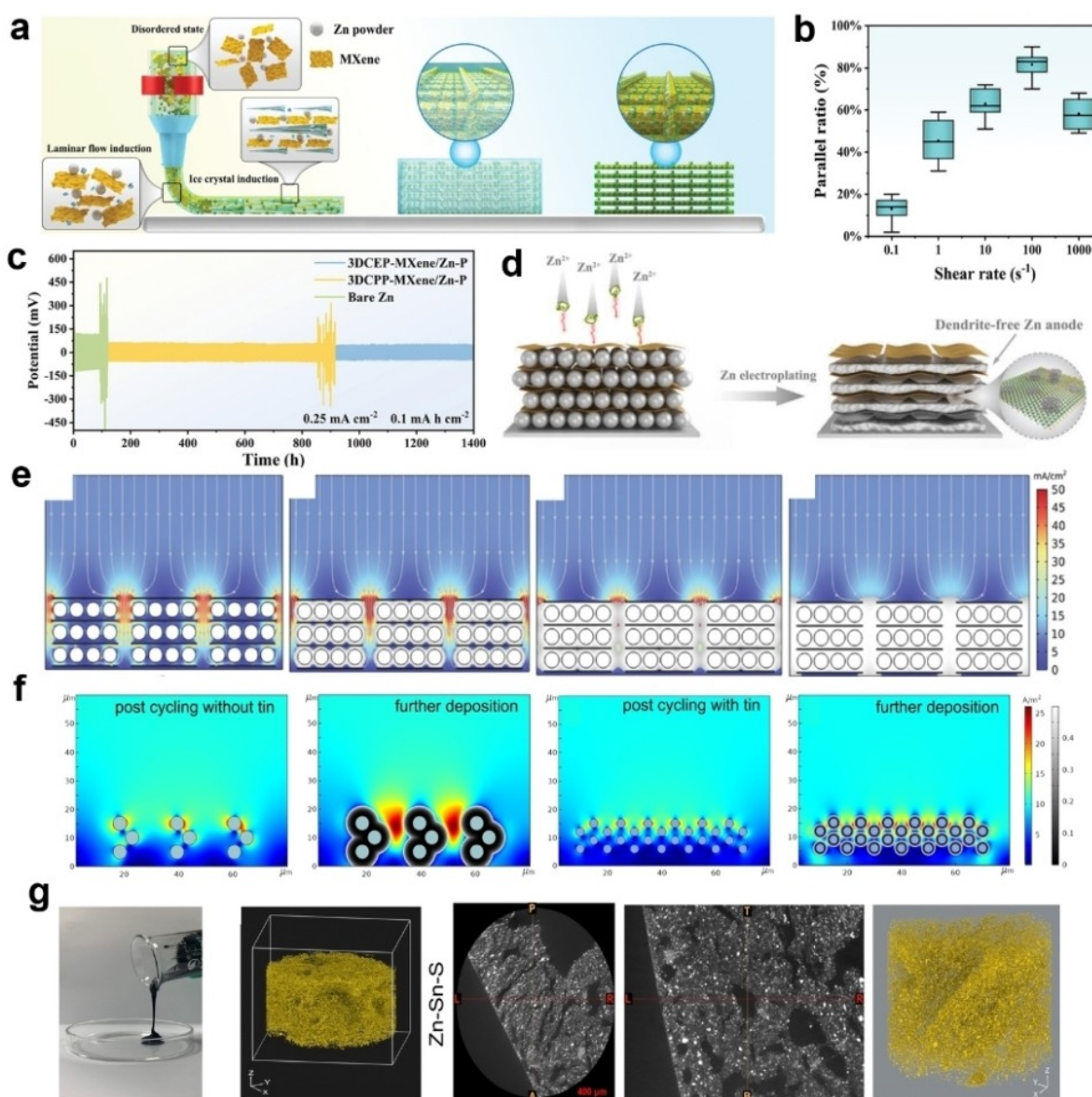


**Figure 7.** a) Schematic diagram of the preparation process of 3DCEP-MXene/Zn−P. b) The relationship between shear rate, MXene content, ink temperature and the parallel ratio of MXene nanosheets. c) Voltage-time profiles of symmetric cells at a current density of 0.25 mA cm$^{-2}$. d) Schematic depiction of Zn deposition behavior on 3DCEP-MXene/Zn−P and 3DCEP−Zn−P anodes. e) COMSOL simulations on 3DCEP-MXene/Zn−P[90] Copyright (2022) John Wiley and Sons. f) COMSOL simulations exhibiting the electric field of zinc deposition in the Zn powder semi-solid slurry anode with and without tin powder after electrochemical cycling. g) X-ray macro-CT images of Zn−Sn−S slurry anode in a half cell after undergoing 20 cycles at 0.5 mAcm$^{-2}$.[41] Copyright (2022) John Wiley and Sons.

Zn powder to construct three-dimensional Zn anode, the $Zn^{2+}$ flux is uniformly distributed. (Figure 7d, e).

## 4.2. Solid and Liquid Composite of Zn Powder Anodes

In recent years, fluid type electrodes have been widely concerned because of their rheological properties similar to liquids, which can effectively alleviate the volume effect of anode materials and inhibit dendrite growth.[93,94] For the first time, Wang et al. reported a semi-solid Zn powder based pulp anode. PAM electrolyte additive added to the anode can delay the corrosion of Zn powder and effectively disperse multi-wall carbon nanotubes in the slurry.[41] In a uniformly dispersed semi-solid slurry, a robust conductive framework is constructed for the Zn powder. In addition, tin powder can be used as a seed to induce uniform deposition of zinc, avoiding zinc agglomeration deposition caused by preferential dissolution of small particles. This has been proved by COMSOL Multiphysics and three-dimensional X-ray micro-computed tomography (CT) (Figure 7f, g). Due to its unique rheological properties, semi-liquid materials are considered as one of the effective methods to mitigate the volume effect of Zn powder anodes during charge and discharge, especially at high current density.[83] As a result, semi-liquid anodes are expected to provide dendrite-free plating behavior similar to the function of liquid metals. On this basis, Zhang et al. successfully prepared a semi-liquid based Zn powder anode (SLA) (Figure 8a).[91] The SLA anode can stably cycle for nearly 450 hours at $5\,mA\,cm^{-2}$ and $5\,mAh\,cm^{-2}$ (Fig-ure 8b, c). In addition to semi-solids, there exist several intermediate states of condensed matter according to the rheological parameters of the Deborah number.[95–98] Viscoelastic solids (i.e., soft solids) are considered to be a promising rheological material for improving electrode properties because they can exhibit high elasticity (solid behavior) while maintaining appropriate viscosity (liquid behavior). Liu et al constructed a soft solid viscoelastic Zn powder composite anode (Figure 8d).[92] Compared with the traditional solid Zn powder anode, the rheological structure of soft solid zinc powder anode imparts a certain liquid behavior, which can accelerate the diffusion of zinc ions in the electrode, uniform $Zn^{2+}$ flux, and inhibit the formation of zinc dendrites. At the same time, the matrix viscosity of the soft solid Zn powder anode is low, and the conductive filler reestablishes the conductive path through diffusion or induced dipole interaction to alleviate the electrical contact problem caused by the volume effect during charge and discharge. The electric field simulation shows that the electric field distribution on the anode surface of ss-ZnP is uniform, therefore, the ss-ZnP anode shows long cycle performance of 400 hours at $5\,mA\,cm^{-2}$ and $5\,mAh\,cm^{-2}$ (Figure 8e). The AFM test further proves that the anode surface of ss-ZnP is flatter than that of s-ZnP anode (Figure 8f). This method contributes to further studies on the design strategies of practical Zn powder anode structures. The various materials synthesized based on the structure optimization strategy and their corresponding electrochemical properties are shown in Table 2.

**Table 2.** Structural optimization strategy for Zn powder anodes.

| Type | Anode | Working Mechanism | Average particle size of Zn powder | Cycle performance | Electrolyte | Full celL performance | Ref |
|---|---|---|---|---|---|---|---|
| 3D Structural optimization | ZnP—MIEC | Regulating the $Zn^{2+}$ flux and anti-corrosion | ~4.3 μm | 100 h at $10\,mA\,cm^{-2}$ | 2 M $ZnSO_4$ | 90% capacity retention after 1500 cycles at $0.5\,A\,g^{-1}$ | [66] |
| | ZCYSM@Zn | Regulating the $Zn^{2+}$ flux and inhibit the volume expansion | / | 4000 h at $10\,mA\,cm^{-2}$ | 3 M $ZnSO_4$ | 80% capacity retention after 5000 cycles at $5\,A\,g^{-1}$ | [69] |
| | ZP-Grad | Optimizes the electric field distribution and regulating the $Zn^{2+}$ flux | ~8.5 μm | 1250 h at $1\,mA\,cm^{-2}$ | 2 M $ZnSO_4$ | 70% capacity retention after 650 cycles at $3\,A\,g^{-1}$ | [70] |
| | 3DP-ZA | Uniform $Zn^{2+}$ deposition | / | 330 h at $1\,mA\,cm^{-2}$ | 3 M Zn-$(OTf)_2$ | 82% capacity retention after 1000 cycles at $1\,A\,g^{-1}$ | [85] |
| | 3D Zn@ZAP | Regulating the $Zn^{2+}$ flux and optimizes the electric field distribution | / | 4700 h at $5\,mA\,cm^{-2}$ | 2 M $ZnSO_4$ | 68% capacity retention after 500 cycles at $1.7\,A\,g^{-1}$ | [86] |
| | 3DCEP MXene/Zn—P | Regulating the $Zn^{2+}$ flux | / | 650 h at $1\,mA\,cm^{-2}$ | 3 M Zn-$(OTf)_2$ | 96% capacity retention after 1600 cycles at $2\,A\,g^{-1}$ | [90] |
| Solid/liquid composite | Zn—Sn—S | Zn nuclei seeds | ~4.91 μm | 300 h at $1\,mA\,cm^{-2}$ | 2 M $ZnSO_4$ | 80% capacity retention after 150 cycles at $1\,A\,g^{-1}$ | [41] |
| | SLA | Regulating the $Zn^{2+}$ flux | / | 450 h at $5\,mA\,cm^{-2}$ | 2 M Zn-$(ClO_4)_2$ | 5000 cycles at $10\,A\,g^{-1}$ | [91] |
| | ss-ZnP | Optimizes the electric field distribution | / | 400 h at $1\,mA\,cm^{-2}$ | 2 M $ZnSO_4$ | 500 cycles at $1\,A\,g^{-1}$ | [92] |
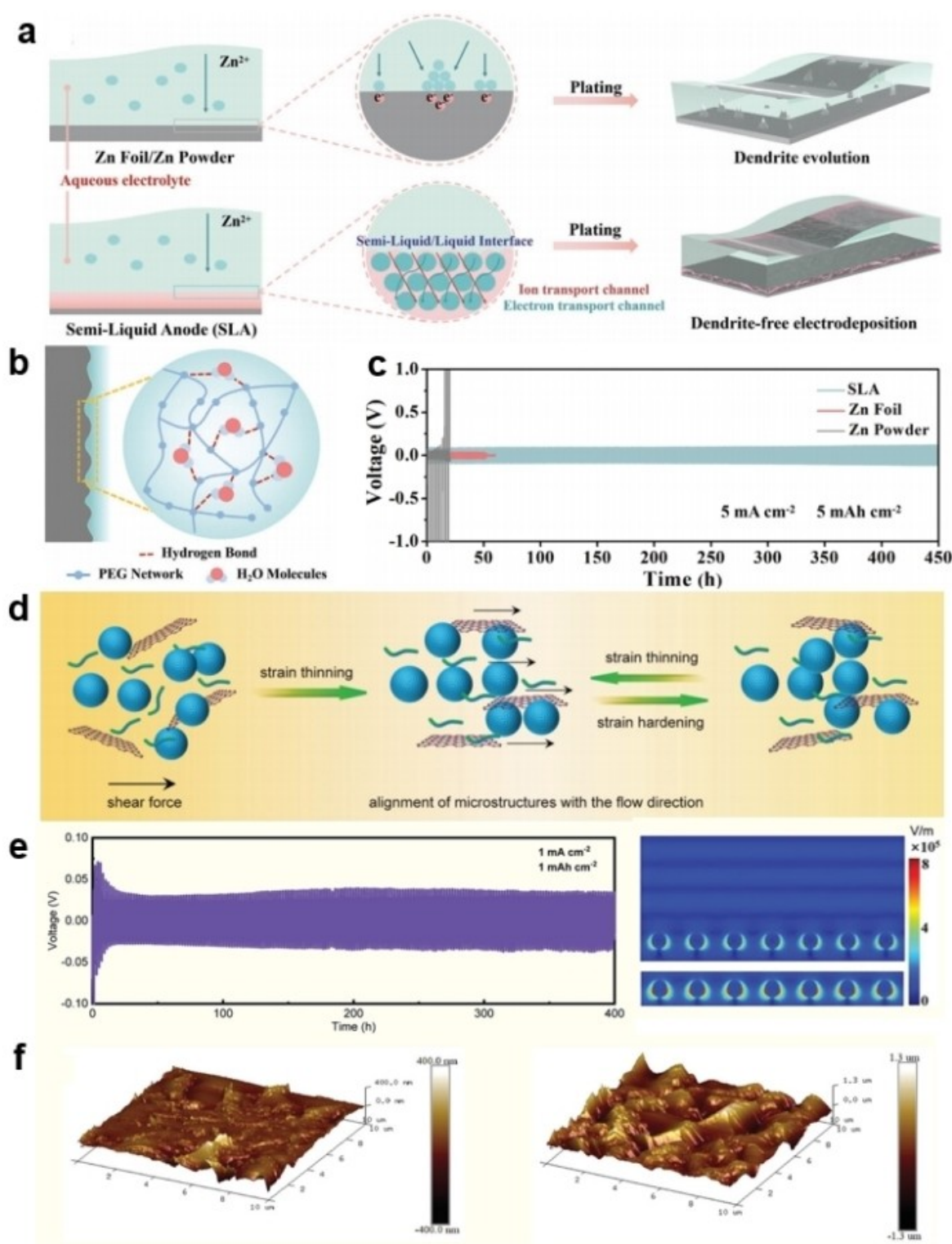
**Figure 8.** a) Schematic diagrams illustrating the morphology evolution of SLA and Zn foil/Zn powder anodes. b) Diagrams demonstrating the formation of hydrogen bond. c) Voltage profiles of a symmetric cell based on SLA.[91] Copyright (2022) John Wiley and Sons. d) Rheological structure of the ss-ZnP anode under different strain amplitudes. e) Voltage-time profiles of symmetric cells at a current density of 1 mA cm$^{-2}$. f) AFM diagrams of ss-ZnP and s-ZnP anodes after 30 cycles at 0.2 mA cm$^{-2}$ with a capacity of 0.2 mAh cm$^{-2}$.[92] Copyright (2023) John Wiley and Sons.

## 5. Summary and Outlook

Owing to their numerous advantages, Zn powder anodes hold considerable promise for applications in the field of energy storage. This paper offers a comprehensive review of the various processing methods of Zn powder anodes that have emerged in recent years. We introduced strategies for structure optimization and surface modification, and summarized the optimization mechanisms of Zn powder anodes, such as the use of Zn–P@In as the crystal seeds for $Zn^{2+}$ ions nucleation, MXene@Zn for inducing uniform zinc deposition, and ss-ZnP for optimizing electric field distribution. We also discussed structural optimization methods such as 3D conductive frames, multi-gradient design, and 3D printing. While Zn powder anodes have immense potential in AZIBs, certain shortcomings in the synthesis methods and commercial applications, need further exploration:

(1) The potential for high zinc utilization rate of Zn powder anodes needs to be explored. Up to now, many excellent works in the field of Zn powder anode research have been reported with unique synthesis methods such as electrostatic self-assembly, 3D printing, bionic structure design and so on. However, the zinc utilization of these Zn powder anodes is generally not high. This prevents them from achieving the energy density competitive with real-world commercial batteries, and each synthesis method carries its own drawbacks. For example, the structure stability of Zn powder anode prepared by electrostatic self-assembly is poor, and the 3D printing inks are subject to temperature gradients. The development of zinc powder anodes that are more suitable for large-scale preparation and can achieve a utilization rate of 80% or higher requires further investigation.

(2) The failure mechanism of Zn powder remains to be thoroughly probed. In situ characterization techniques can be used to monitor the degree of hydrogen evolution of Zn powder and observe the volume change of Zn powder during deposition/dissolution. Most existing reports correlate the mechanism of action with observation of Zinc powder deposition structure over a relatively short time range, hence the failure mechanism of Zn powder and the action principles of modification methods can be deeply analyzed by combining in situ characterization technology and theoretical simulation.

(3) A combination of strategies should be considered. Most strategies that address existing issues with Zn powder anodes involve single modification strategy for the surface and structure of zinc anodes. A combination of various strategies can comprehensively improve the battery performance to meet the practical application needs of zinc-ion batteries. For example, the utilization of electrolyte additives can effectively mitigate the water-induced corrosion of zinc powder anodes. Therefore, integrating this approach with the aforementioned strategies for structural optimization (such as constructing a conductive framework) represents a promising avenue for realizing practical Zn powder anodes.

## Conflict of Interests

The authors declare no conflict of interest.

## Data Availability Statement

The data that support the findings of this study are available from the corresponding author upon reasonable request.

[1] X. Jia, C. Liu, Z. Neale, J. Yang, G. Cao, *Chem. Rev.* **2020**, *120*, 7795–7866.
[2] Z. Yi, G. Chen, F. Hou, L. Wang, J. Liang, *Adv. Energy Mater.* **2020**, *11*, 2003065.
[3] F. Chang, W. Gao, J. Guo, P. Chen, *Adv. Mater.* **2021**, *33*, 2005721.
[4] W. Braff, J. Mueller, J. Trancik, *Nat. Clim. Change.* **2016**, *6*, 964–969.
[5] T. Szkopek, *Nat. Nanotechnol.* **2021**, *16*, 853–854.
[6] L. Yuan, J. Hao, C. Kao, C. Wu, H. Liu, S. Dou, S. Qiao, *Energy Environ. Sci.* **2021**, *14*, 5669–5689.
[7] R. Amal, H. Zhao, D. Wang, L. Wang, *Adv. Energy Mater.* **2017**, *7*, 1703091.
[8] Y. Lv, Y. Xiao, L. Ma, C. Zhi, S. Chen, *Adv. Mater.* **2021**, *34*, 2106409.
[9] L. Blanc, D. Kundu, L. Nazar, *Joule.* **2020**, *4*, 771–799.
[10] J. Chen, W. Zhao, J. Jiang, X. Zhao, S. Zheng, Z. Pan, X. Yang, *Energy Storage Mater.* **2023**, *59*, 102767.
[11] C. Zhu, P. Li, G. Xu, H. Cheng, G. Gao, *Coord. Chem. Rev.* **2023**, *485*, 1.
[12] J. Song, K. Xu, N. Liu, D. Reed, X. Li, *Mater. Today* **2021**, *45*, 191–212.
[13] J. Feng, D. Zheng, R. Yin, X. Niu, X. Xu, S. Meng, S. Ma, W. Shi, F. Wu, W. Liu, X. Cao, *Small Structures* **2023**, *4*, 2200323.
[14] G. Fang, J. Zhou, A. Pan, S. Liang, *ACS Energy Lett.* **2018**, *3*, 2480–2501.
[15] T. Wang, C. Li, X. Xie, B. Lu, Z. He, S. Liang, J. Zhou, *ACS Nano* **2020**, *14*, 16321–16347.
[16] N. Zhang, X. Chen, M. Yu, Z. Niu, F. Cheng, J. Chen, *Chem. Soc. Rev.* **2020**, *49*, 4203–4219.
[17] J. Ming, J. Guo, C. Xia, W. Wang, H. Alshareef, *Mat. Sci. Eng. R* **2019**, *135*, 58–84.
[18] W. Hu, J. Ju, N. Deng, M. Liu, W. Liu, Y. Zhang, L. Fan, W. Kang, B. Cheng, *J. Mater. Chem. A* **2021**, *9*, 25750–25772.
[19] C. Nie, G. Wang, D. Wang, M. Wang, X. Gao, Z. Bai, N. Wang, J. Yang, Z. Xing, S. Dou, *Adv. Energy Mater.* **2023**, *13*, 2300606.
[20] J. Zheng, Z. Huang, F. Ming, Y. Zeng, B. Wei, Q. Jiang, Z. Qi, Z. Wang, H. Liang, *Small* **2022**, *18*, 2200006.
[21] H. Liu, Q. Ye, D. Lei, Z. Hou, W. Hua, Y. Huyan, N. Li, C. Wei, F. Kang, J. Wang, *Energy Environ. Sci.* **2023**, *16*, 1610–1619.
[22] X. Xu, Y. Chen, D. Liu, D. Zheng, X. Dai, W. Shi, X. Cao, *Chem. Rec.* **2022**, *22*, e202200079.
[23] Z. Cao, P. Zhuang, X. Zhang, M. Ye, J. Shen, P. Ajayan, *Adv. Energy Mater.* **2020**, *10*, 2001599.
[24] Q. Zhang, J. Luan, Y. Tang, X. Ji, H. Wang, *Angew. Chem. Int. Ed.* **2020**, *59*, 13180–13191.

[25] X. Xu, Y. Chen, D. Zheng, P. Ruan, Y. Cai, X. Dai, X. Niu, C. Pei, W. Shi, W. Liu, F. Wu, Z. Pan, H. Li, X. Cao, *Small* **2021**, *17*, e2101901.

[26] X. Fan, H. Yang, B. Feng, Y. Zhu, Y. Wu, R. Sun, L. Gou, J. Xie, D. Li, Y. Ding, *Chem. Eng. J.* **2022**, *445*, 136799.

[27] S. Wang, Q. Ran, R. Yao, H. Shi, Z. Wen, M. Zhao, X. Lang, Q. Jiang, *Nat. Commun.* **2020**, *11*, 1634.

[28] Y. Song, P. Ruan, C. Mao, Y. Chang, L. Wang, L. Dai, P. Zhou, B. Lu, J. Zhou, Z. He, *Nano-Micro Lett.* **2022**, *14*, 218.

[29] Y. Lin, Y. Hu, S. Zhang, Z. Xu, T. Feng, H. Zhou, M. Wu, *ACS Appl. Energy Mater.* **2022**, *5*, 15222–15232.

[30] Q. Li, Y. Wang, F. Mo, D. Wang, G. Liang, Y. Zhao, Q. Yang, Z. Huang, C. Zhi, *Adv. Energy Mater.* **2021**, *11*, 2003931.

[31] W. Du, S. Huang, Y. Zhang, M. Ye, C. Li, *Energy Storage Mater.* **2022**, *45*, 465–473.

[32] Z. Xu, Y. Li, G. Li, H. Zhang, X. Wang, *Matter* **2023**, *6*, 3075–3086.

[33] F. Wu, Y. Chen, Y. Chen, R. Yin, Y. Feng, D. Zheng, X. Xu, W. Shi, W. Liu, X. Cao, *Small* **2022**, *18*, 2202363.

[34] C. Cao, W. Du, C. Li, M. Ye, Y. Zhang, Y. Tang, X. Liu, *J. Mater. Chem. A* **2023**, *11*, 14345–14355.

[35] Q. Li, S. Tang, R. Luo, P. Wei, P. Chen, J. Cong, G. Liu, Z. Liu, Y. Gou, H. Wu, S. Sun, J. Han, Y. Shi, C. Fang, C. Yan, *Energy Storage Mater.* **2024**, *66*, 103229.

[36] J. Parker, C. Chervin, Nelson, Chervin, D. Rolison, J. Long, *Energy Environ. Sci.* **2014**, *7*, 1117–1124.

[37] V. Yufit, F. Tariq, D. Eastwood, M. Biton, B. Wu, P. Lee, N. Brandon, *Joule* **2019**, *3*, 485–502.

[38] B. Tang, L. Shan, S. Liang, J. Zhou, *Energy Environ. Sci.* **2019**, *12*, 3288–3304.

[39] X. Li, Q. Li, Y. Hou, Q. Yang, Z. Chen, Z. Huang, G. Liang, Y. Zhao, L. Ma, M. Li, Q. Huang, C. Zhi, *ACS Nano* **2021**, *15*, 14631–14642.

[40] J. Wu, X. Shen, H. Zhou, X. Li, H. Gao, J. Ge, T. Xu, H. Zhou, *Small* **2023**, 2308541.

[41] Z. Yang, Q. Zhang, W. Li, C. Xie, T. Wu, C. Hu, Y. Tang, H. Wang, *Angew. Chem. Int. Ed.* **2023**, *62*, e202215306.

[42] C. Tan, X. Cao, X. Wu, Q. He, J. Yang, X. Zhang, J. Chen, W. Zhao, S. Han, G. Nam, M. Sindoro, H. Zhang, *Chem. Rev.* **2017**, *117*, 6225–6331.

[43] Y. An, Y. Tian, C. Liu, S. Xiong, J. Feng, Y. Qian, *ACS Nano* **2021**, *15*, 15259–15273.

[44] N. Zhang, S. Huang, Z. Yuan, J. Zhu, Z. Zhao, Z. Niu, *Angew. Chem. Int. Ed.* **2020**, *60*, 2861–2865.

[45] Y. Zhang, Z. Cao, S. Liu, Z. Du, Y. Cui, J. Gu, Y. Shi, B. Li, S. Yang, *Adv. Energy Mater.* **2022**, *12*, 2103979.

[46] J. Zhou, M. Xie, F. Wu, Y. Mei, Y. Hao, R. Huang, G. Wei, A. Liu, L. Li, R. Chen, *Adv. Mater.* **2021**, *33*, 2101649.

[47] B. Wu, B. Guo, Y. Chen, Y. Mu, H. Qu, M. Lin, J. Bai, T. Zhao, L. Zeng, *Energy Storage Mater.* **2023**, *54*, 75–84.

[48] M. Qiu, H. Jia, H. Liu, B. Tawiah, S. Fu, *J. Alloys Compd.* **2022**, *891*, 161886.

[49] A. Bayaguud, X. Luo, Y. Fu, C. Zhu, *ACS Energy Lett.* **2020**, *5*, 3012–3020.

[50] Q. Zhang, J. Luan, L. Fu, S. Wu, Y. Tang, X. Ji, H. Wang, *Angew. Chem. Int. Ed.* **2019**, *58*, 15841–15847.

[51] M. Yan, N. Dong, X. Zhao, Y. Sun, H. Pan, *ACS Energy Lett.* **2021**, *6*, 3236–3243.

[52] Y. Jin, K. Han, Y. Shao, M. Sushko, J. Xiao, H. Pan, J. Liu, *Adv. Funct. Mater.* **2020**, *30*, 2003932.

[53] X. Cai, X. Wang, Z. Bie, Z. Jiao, Y. Li, W. Yan, H. Fan, W. Song, *Adv. Mater.* **2023**, *36*, DOI: 10.1002/adma.202306734.

[54] B. Li, S. Liu, Y. Geng, C. Mao, L. Dai, L. Wang, S. Jun, B. Lu, Z. He, J. Zhou, *Adv. Funct. Mater.* **2024**, *34*, 2214033.

[55] T. Wang, P. Wang, L. Pan, Z. He, L. Dai, L. Wang, S. Liu, S. Jun, B. Lu, S. Liang, J. Zhou, *Adv. Energy Mater.* **2023**, *13*, 2203523.

[56] X. Huyan, Z. Yi, Z. Sang, S. Tan, J. Liu, R. Chen, W. Si, J. Liang, F. Hou, *Appl. Surf. Sci.* **2023**, *614*, 156209.

[57] J. Dong, H. Peng, J. Wang, C. Wang, D. Wang, N. Wang, W. Fan, X. Jiang, J. Yang, Y. Qian, *Energy Storage Mater.* **2023**, *54*, 875–884.

[58] A. Li, M. Chen, Q. Tian, X. Han, J. Chen, *J. Alloys Compd.* **2023**, *965*, 171337.

[59] M. Cui, Y. Xiao, L. Kang, W. Du, Y. Gao, X. Sun, Y. Zhou, X. Li, H. Li, F. Jiang, C. Zhi, *ACS Appl. Energ. Mater.* **2019**, *2*, 6490–6496.

[60] Y. Zhang, G. Wang, F. Yu, G. Xu, Z. Li, M. Zhu, Z. Yue, M. Wu, H. Liu, S. Dou, C. Wu, *Chem. Eng. J.* **2021**, *416*, 128062.

[61] A. Naveed, A. Ali, T. Rasheed, X. Wang, P. Ye, X. Li, Y. Zhou, S. Mingru, Y. Liu, *J. Power Sources* **2022**, *525*, 231122.

[62] J. Yan, J. Yu, B. Ding, *Adv. Mater.* **2018**, *30*, 1705105.

[63] X. Shen, G. Zhao, L. Fan, Z. Guo, C. Zhao, A. Chen, G. Yang, Z. Cheng, N. Zhang, *J. Mater. Chem. A* **2020**, *8*, 21961–21967.

[64] M. Wang, J. Wolfenstine, J. Sakamoto, *Adv. Funct. Mater.* **2020**, *30*, 1909140.

[65] W. Guo, S. Liu, X. Guan, X. Zhang, X. Liu, J. Luo, *Adv. Energy Mater.* **2019**, *9*, 1900193.

[66] M. Zhang, P. Yu, K. Xiong, Y. Wang, Y. Liu, Y. Liang, *Adv. Mater.* **2022**, *34*, e2200860.

[67] H. Liu, J. Li, D. Wei, X. Liu, Z. Cai, H. Zhang, Z. Lv, L. Chen, H. Li, H. Luo, Y. Zhao, H. Yu, X. Wang, F. Chen, G. Zhang, H. Duan, *Adv. Funct. Mater.* **2023**, *33*, 2300419.

[68] C. Jo, N. Voronina, Y. Sun, S. Myung, *Adv. Mater.* **2021**, *33*, 2006019.

[69] Q. Hu, J. Hou, Y. Liu, L. Li, Q. Ran, J. Mao, X. Liu, J. Zhao, H. Pang, *Adv. Mater.* **2023**, *35*, e2303336.

[70] X. Zhao, Y. Gao, Q. Cao, F. Bu, J. Pu, Y. Wang, C. Guan, *Adv. Energy Mater.* **2023**, *13*, 2301741.

[71] J. Yang, L. Liu, Z. Yu, P. Chen, J. Li, P. Dananjaya, E. Koh, W. Lew, K. Liu, P. Yang, H. Fan, *ACS Energy Lett.* **2023**, *8*, 2042–2050.

[72] G. Liang, J. Zhu, B. Yan, Q. Li, A. Chen, Z. Chen, X. Wang, B. Xiong, J. Fan, J. Xu, C. Zhi, *Energy Environ. Sci.* **2022**, *15*, 1086–1096.

[73] Q. Cao, Y. Gao, J. Pu, X. Zhao, Y. Wang, J. Chen, C. Guan, *Nat. Commun.* **2023**, *14*, 641.

[74] H. He, L. Zeng, D. Luo, J. He, X. Li, Z. Guo, C. Zhang, *Adv. Mater.* **2023**, *35*, 2211498.

[75] T. Wang, J. Duan, B. Zhang, W. Luo, X. Ji, H. Xu, Y. Huang, L. Huang, Z. Song, J. Wen, C. Wang, Y. Huang, J. Goodenough, *Energy Environ. Sci.* **2022**, *15*, 1325–1333.

[76] D. McOwen, S. Xu, Y. Gong, Y. Wen, G. Godbey, J. Gritton, T. R. Hamann, J. Dai, G. Hitz, L. Hu, E. Wachsman, *Adv. Mater.* **2018**, *30*, 1707132.

[77] J. Hu, Y. Jiang, S. Cui, Y. Duan, T. Liu, H. Guo, L. Lin, Y. Lin, J. Zheng, K. Amine, F. Pan, *Adv. Energy Mater.* **2016**, *6*, 1600856.

[78] J. Qian, Q. Chen, M. Hong, W. Xie, S. Jing, Y. Bao, G. Chen, Z. Pang, L. Hu, T. Li, *Mater. Today* **2022**, *54*, 18–26.

[79] S. Praveen, G. Sim, C. Ho, C. Lee, *Energy Storage Mater.* **2021**, *41*, 748–757.

[80] T. Wei, B. Ahn, J. Grotto, J. Lewis, *Adv. Mater.* **2018**, *30*, 1703027.

[81] J. Wang, Q. Sun, X. Gao, C. Wang, W. Li, F. B. Holness, M. Zheng, R. Li, A. Price, X. Sun, T. Sham, X. Sun, *ACS Appl. Mater. Interfaces* **2018**, *10*, 39794–39801.

[82] A. Ambrosi, M. Pumera, *Chem. Soc. Rev.* **2016**, *45*, 2740–2755.

[83] K. Fu, Y. Yao, J. Dai, L. Hu, *Adv. Mater.* **2016**, *29*, 1603486.

[84] X. Gao, X. Zheng, X. Yang, R. Sun, J. Zhang, X. Sun, *Mater. Today* **2022**, *59*, 161–181.

[85] L. Zeng, J. He, C. Yang, D. Luo, H. Yu, H. He, C. Zhang, *Energy Storage Mater.* **2023**, *54*, 469–477.

[86] J. Yang, X. Xu, Y. Gao, Y. Wang, Q. Cao, J. Pu, F. Bu, T. Meng, C. Guan, *Adv. Energy Mater.* **2023**, *13*, 2301997.

[87] M. Saadi, A. Maguire, N. Pottackal, M. Thakur, M. Ikram, A. Hart, P. Ajayan, M. Rahman, *Adv. Mater.* **2022**, *34*, 2108855.

[88] J. Bae, S. Oh, B. Lee, C. Lee, J. Chung, J. Kim, S. Jo, S. Seo, J. Lim, S. Chung, *Energy Storage Mater.* **2023**, *57*, 277–288.

[89] C. Zhu, N. Schorr, Z. Qi, B. Wygant, D. Turney, G. Yadav, M. A. Worsley, E. Duoss, S. Banerjee, E. Spoerke, A. van Buuren, T. Lambert, *Small Structures* **2022**, *4*, 2200323.

[90] H. Lu, J. Hu, Y. Zhang, K. Zhang, X. Yan, H. Li, J. Li, Y. Li, J. Zhao, B. Xu, *Adv. Mater.* **2023**, *35*, e2209886.

[91] Q. Liu, Z. Yu, R. Zhou, B. Zhang, *Adv. Funct. Mater.* **2022**, *33*, 2210290.

[92] C. Cao, K. Zhou, W. Du, C. Li, M. Ye, Y. Zhang, Y. Tang, X. Liu, *Adv. Energy Mater.* **2023**, *13*, 2301835.

[93] Y. Zhang, Z. Han, Z. Huang, C. Zhang, C. Luo, G. Zhou, W. Lv, Q. Yang, *ACS Energy Lett.* **2021**, *6*, 3761–3768.

[94] G. Soloveichik, *Chem. Rev.* **2015**, *115*, 11533–11558.

[95] S. Kenney, K. Poper, G. Chapagain, G. Christopher, *Rheol. Acta* **2013**, *52*, 485–497.

[96] P. de Souza Mendes, *J. Non-Newtonian Fluid Mech.* **2007**, *147*, 109–116.

[97] M. De Corato, G. D'Avino, *Soft Matter* **2017**, *13*, 196–211.

[98] M. Villone, G. D'Avino, M. Hulsen, F. Greco, P. Maffettone, *J. Non-Newtonian Fluid Mech.* **2013**, *195*, 1–8.